

June 2020

Monitoring CO₂ underground storage with the
Riccati equation

Paper no. 3

Cand. Real. Knut Sørdsal

Norway, 2020

Abstract

A study is made of an inversion technique of the Riccati type applied to a CO₂-plume on the Sleipner field in the North sea. This paper employs Q-models to introduce forward and inverse filtering of the data. The solution of the Riccati equation with the the Kolsky-Wang Q-model has been presented in previous papers and is applied here. The linear solution of the wave equation introducing attenuation and dispersion has been studied by Wang. He used a modification of Kolsky's Q-model and applied it on a downward continuation algorithm. I have taken the theory further with a general Q-model and a more elegant inversion. The theory is applied on real seismic data from the Sleipner field.

Higher amounts of CO₂ in the atmosphere has contributed to finding techniques to mitigate the emissions of CO₂. One of those techniques is Carbon Capture and Storage (CCS). CO₂ can be stored in subsurface reservoirs over time. Monitoring and modeling of reservoirs is important to avoid leakage and to predict how the CO₂ could migrate. Modeling is also useful when the seismic interpreter needs a close look at the subsurface data. Then seismic from modeling with known parameters can be useful. I have used the Riccati-equation both for modeling and for inversion to recover the original data used in the seismic theory.

I will connect my theory to real data, and the first place in the world to inject CO₂ was in the Sleipner field in the Norwegian North Sea. The injection found place in 1996 in the Sleipner East field into the Utsira formation. The reservoir is estimated to have a vertical thickness about 200 m at the injection point, and the estimated caprock for the CO₂ is about 100 m thick.

So, this article shows modeling of the seismic response from different synthetic models associated with CO₂ underground storage where the parameters are based on real data.

CO₂ saturation, geometry of the models and some other things are all important parameters affecting the seismic result. I have done calculations with a background model that is saturated with CO₂ and received different results depending on saturation percent. Parts of the text about the Sleipner field is taken from a thesis by Nordahl (2015).

Carbon capture and storage

Carbon capture and storage (CCS) subsurface is one technique to help reduce the amount of CO₂ emissions to the atmosphere. Use of fossil fuels for power generations will increase the amount of CO₂ emissions, but capture of CO₂ in the produced natural gas will help mitigate the emissions. When the CO₂ is captured and stored in subsurface reservoirs it is important to monitor the behavior of the CO₂ plume. Monitoring of subsurface seismic amplitudes is important to avoid leakage of CO₂ into the sea and atmosphere and to monitor how the plume will develop over time. The primary objective for this paper is to get a better understanding of seismic amplitude anomalies associated with subsurface storage of CO₂ over time. Several models with varying size of the plume and different saturation of CO₂ will be created.

The models are hypothetical, but the whole background model is based on data from the CO₂ injection site in order to get a realistic setting of the modeling.

This paper will both introduce seismic modeling and inversion. Seismic modeling is important in the seismic data acquisition process to give the best possible results considering what the main target is. If the seismic interpreter has problems interpreting the real data, synthetic seismic with known properties can be used for comparison. With modeling, it is possible to test different survey parameters, like spacing of the shots/receivers, frequencies and different offsets. All these parameters will play a vital role in the resulting seismic and I will study the effect of absorption that is introduced as forward Q-filtering. (FQF)

Inversion is an attempt to use modeled data to recover the original data that is consistent with real data. The effect of recovering for absorption is called inverse Q-filtering. (IQF).

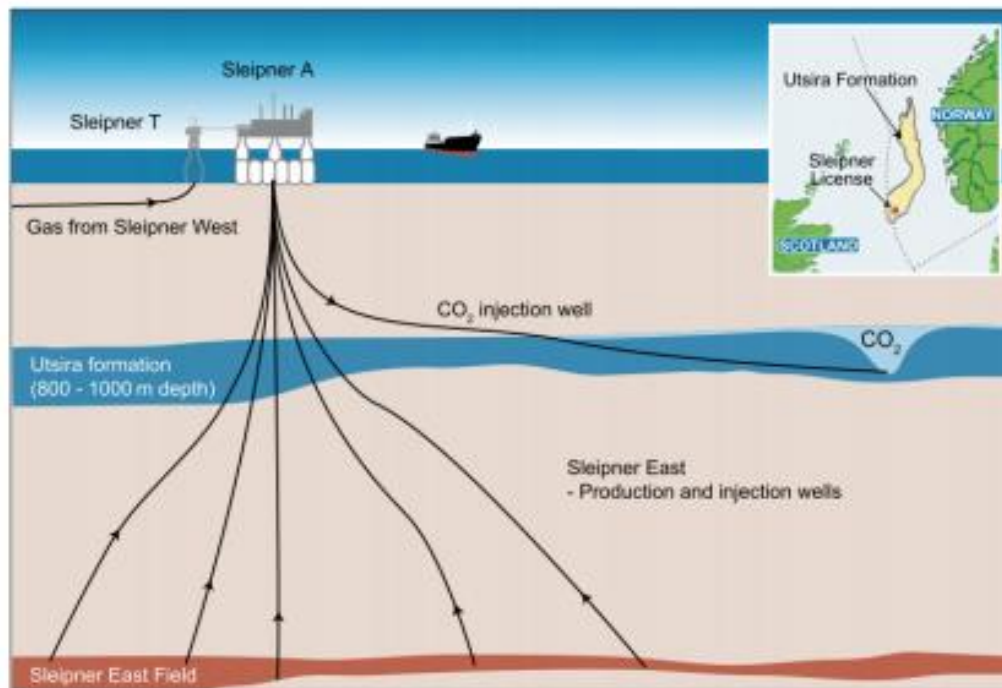


Figure 1: Utsira formation (from IPCC 2005)

The following text will shortly describe the geology of the areas where we find the Sleipner fields (both east and west) and facts about the CO₂-reservoir and the caprock. The first injection of CO₂ found place in 1996 at the Sleipner East field (Arts et al., 2004a), as the first injection plant in the world to help mitigate the CO₂ emissions.

The Sleipner field is located in the Norwegian North Sea (Figure 1) and in an area called Southern Viking Graben. The Viking Graben is formed by rifting in the Late Jurassic to Early Cretaceous where the rifting led to rapid sedimentation of shale under an anoxic environment. The result is several known and large hydrocarbon fields, and one of them is Sleipner (Karstens and Berndt, 2015).

The Utsira sand is varying in thickness between 200 and 300 m (Chadwick et al., 2004a), and is about 200 m thick around the injection point and consist of deltaic sand material (Halland et al., 2011). The sand is approximately about 820-1030 m below sea-level (Ghaderi and Landrø, 2009). Due to the marine depositional environment the sand package consist of thin layer of shale in between, ranking from 1-1,5 m thick. About 20 m below the top of the reservoir we find a thicker shale layer, about 5-7 m thick (Figure 1.2) (Arts et al., 2004a). From the well logs (Figure 1.2), we observe the Utsira sand to be closer to 300 m thick. The gamma ray log from Sleipner East at the injection site (Figure 2 bottom) shows the thin shale layer in the Utsira formation. Gamma ray measures the amount of radioactive material like thorium, uranium and potassium. Shale and source rock material have higher content of these materials than clean sandstone (Rafaelsen, 2013). To be a good storage reservoir the sand must be of high porosity and permeability, and have a huge storage capacity. The Utsira sand fills all this qualifications.

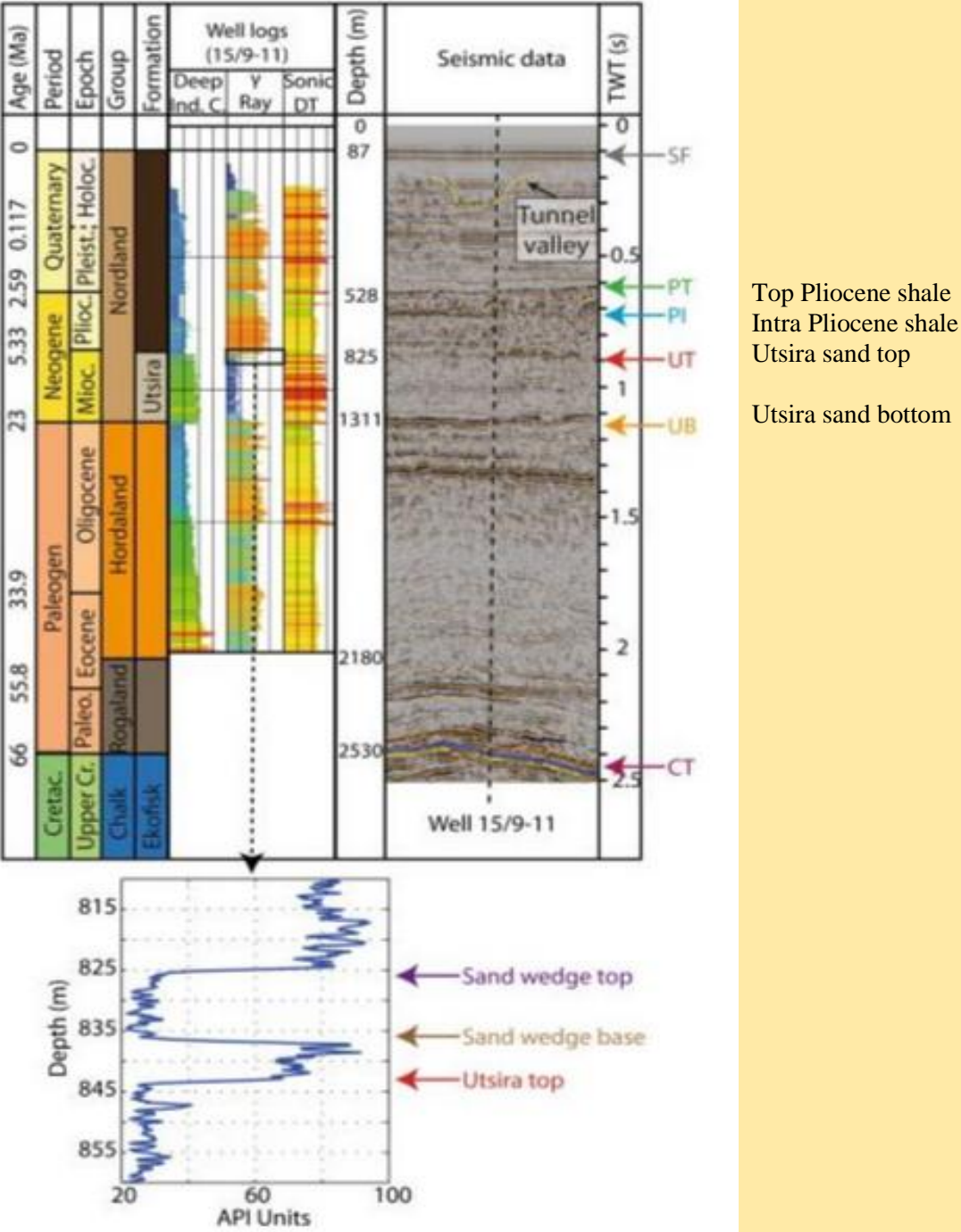


Figure 2 The uppermost picture: Geologic time scale, well logs and 2D section of seismic from the area from (Karstens and Berndt, 2015). Lowermost picture: A closer view of the gamma ray response right above the Utsira top showing the presence of the sand wedge. Modified from (Karstens and Berndt, 2015).

The formation known as the caprock of the CO₂ reservoir is from Pliocene age in the Nordland group, also called the Nordland shale. The unit known as the Nordland shale (Pliocene shale) was deposited in a deep marine environment resulting in a lower permeable mudstones with sand in between (Karstens and Berndt, 2015). The unit assumed to be the immediate caprock of the reservoir is about 50-100 m thick, and consist of silty mudstone. The unit above the caprock is coarsening upwards (Chadwick et al., 2004a).

From the well 15/9-11 (Figure 2 right) one can observe a thicker unit (11m) of sand above the Utsira sand, in the Nordland group. It is a 8 m thick package of mudstone between the Utsira sand and the 11m sand wedge. Above this sand wedge is the rest of the package known as Nordland shales (Karstens and Berndt, 2015).

Figure 3 shows a section from the well 15/9 -11 corresponding to the notations to the right on fig 2.

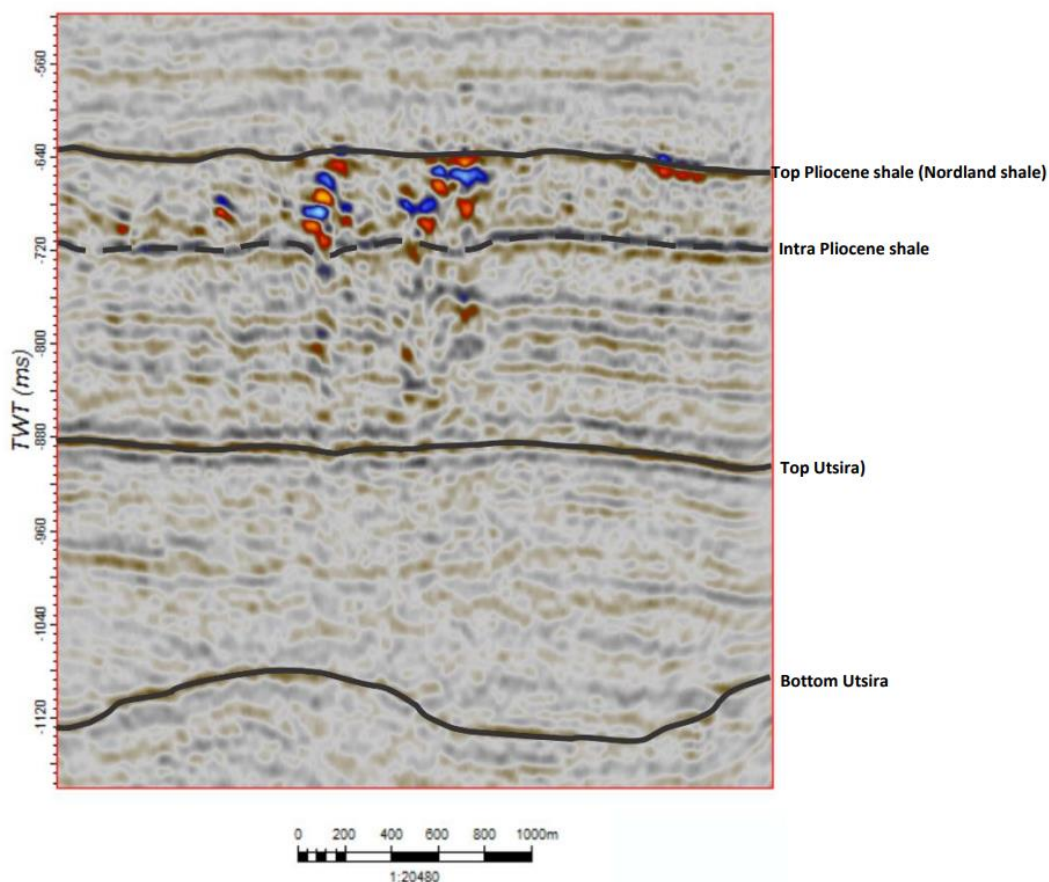


Figure 3 shows that the reflection from Utsira bottom is irregular. The features observed is interpreted to be mounds as a result of the underlying mudstone in the Hordaland group (Figure 2) (Karstens and Berndt, 2015).

Figure 3 shows seismic amplitude anomalies as bright spots in the sand wedge, Utsira sand, and the Pliocene shale. We know that one can only observe that the Utsira bright spots only occur in the north-east part of the study area, and is not detected above Sleipner East where the injection happens. The bright spots in the Utsira occur close to the top of the formation and is interpreted to be gas accumulations (Karstens and Berndt, 2015). The bright spots in the sand wedge is interpreted to be gas accumulations, same as in the Utsira Sand. Further one can observe an intra-reservoir shale reflection within the Pliocene shale. Above this reflection, is it seismic anomalies that are chaotic. The same type

of anomaly is observed in the Pliocene shale as observed in the sand wedge and the Utsira Sand. Some narrow pipe structures are also visible (Karstens and Berndt, 2015).

Other anomalies observed in Figure 3 are type A-anomalies, B-anomalies and C-anomalies. They are recognized respectively as high amplitude vertical reflections, chaotic seismic amplitudes and elongated amplitudes.

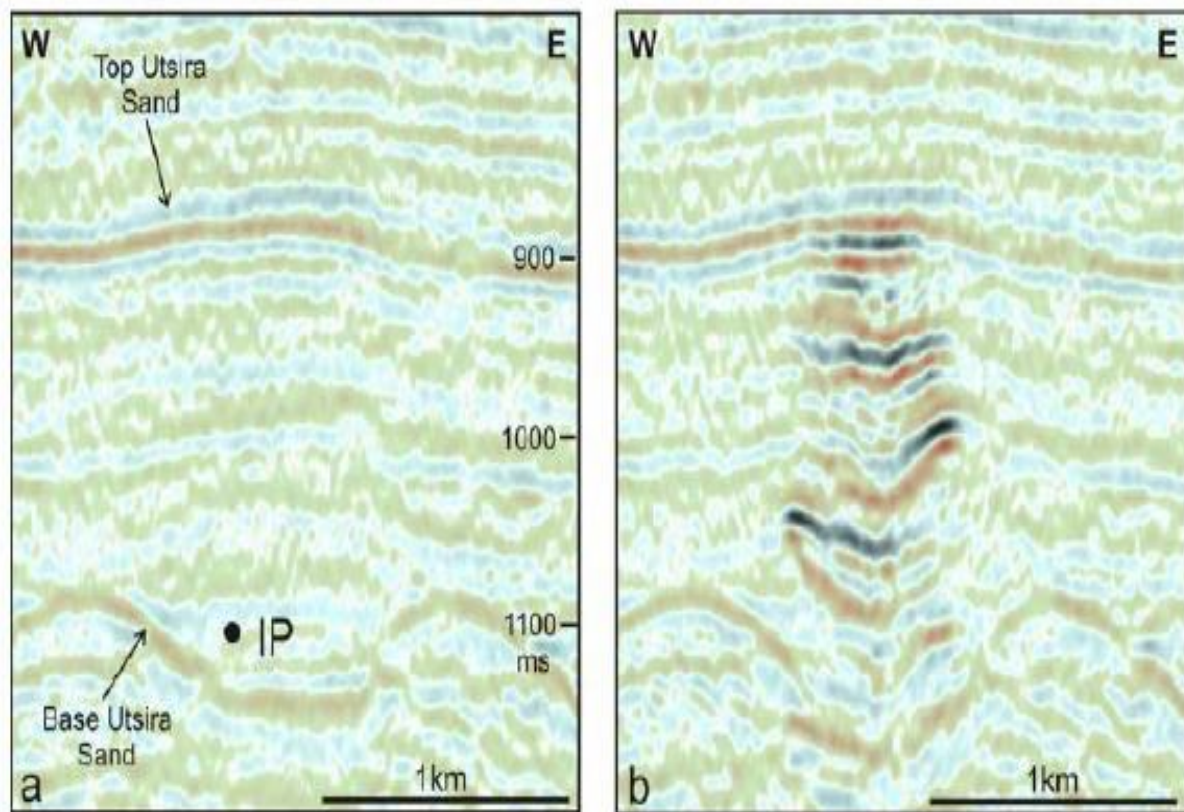


Fig.4. CO₂ layers from Utsira sand, Sleipner field

So, both to sum up, and introduce some more details: the Sleipner East field in the North Sea is located 250 km from the coast of Norway (IPCC, 2005). Sleipner East is producing gas/condensate and Sleipner West is producing natural gas, both with Equinor as an operator. The concentrations of CO₂ in the natural gas is too high at the Sleipner West field, so they separate the CO₂ from the gas before the CO₂ is transported by pipeline to the Sleipner East field for injection. Normally they would release the CO₂ into the atmosphere, but in 1991 the Norwegian government implemented tax on the CO₂ emissions.

Due to this Equinor and the Sleipner partners started injecting CO₂ both due to economic and environmental reasons in 1996. The water depth at the injections site is about 80 m (Ghaderi and Landrø, 2009) and the injection point is 1010-1013 m below sea level (Arts et al., 2004a). The injection rate is around 1 million tonnes per year and the goal is to store 20 million tonnes (Chadwick et al., 2004a).

Introduction to seismic

I will now introduce seismic that is used to monitor the field. Since CO₂ tends to migrate upward the subsurface, it is important to watch carefully the behavior of the plume in the study area. I will, as mentioned in the introduction, concentrate on the effect of absorption that is introduced as forward Q-filtering. Seismic inverse Q-filtering (IQF) is one sector of regular inversion techniques that employs a

wave propagation reversal procedure that compensates for energy absorption and corrects wavelet distortion due to velocity dispersion. When modelling for the inversion we introduce forward Q-filtering (FQF) models, and will give a short description of the background for such models.

Actually, there is a wide range of mathematical definitions of the Q-model presented in the literature, and Wang (2008) summed up about this. A good start is the Kolsky (1953) model that is used extensively in Q-filtering. Wang proposed to modify the Kolsky's basic attenuation-dispersion model. This was primarily an attempt to accurately represent the velocity dispersion effect within the seismic frequency band.

Wang writes that if one compares the basic Kolsky model with other different mathematical Q models, one finds that different models were not close to the basic Kolsky model. Wang, by using a modified Kolsky model, was able to derive a set of analytically derived parameters. The primary goal was to make Kolsky's model comparative with a model satisfying a dispersion condition that is necessary to preserve the causality of a propagating wavelet. Such a dispersion relation is called the Kramers-Krönig dispersion relation. A model of this kind has been discussed by Futterman (1962).

I will use Wang's modification of Kolsky in this article. However, to avoid a rather complicated inverse theory, I will use a least square (LSQ) solution in the Riccati inversion to replace Wang's inverse Q-filtering theory with downward continuation. An attempt with this inversion method without the LSQ-solution was done by Gjevik et al. (1975). In another article Nilsen and Gjevik (1978) presented the theory in a broader way and one absorption model was included. Their theory has been further developed and was presented in two papers on Researchgate. (Sørdsal (2018), Sørdsal (2019)).

Basics of modelling with absorption included

Inverse Q-filtering algorithms are mainly based on forward wave propagation migration type approach. Then the decay of the frequency content due to absorption can be inspected at each time sample. (Wang (2008).) Following Gjevik we can assume monochromatic plane-waves propagating along a vertical axis. Let P define the stress (pressure) and W the displacement. Density is ρ . Newton's second law gives:

$$\frac{dP}{dz} + \rho\omega^2 W = 0 \quad (1)$$

Correspondingly, a stress-strain relationship of the following form is assumed (Hook's law):

$$P = \rho v_r^2 Y \frac{dW}{dz} \quad (2)$$

In Eq.(2) v_r is the reference velocity which could be taken as the group velocity in case of dispersion. The function Y represents depth and frequency-dependent absorption.

In case of no damping, $Y=1$ and Eq.(2) is simply Hookes law.

Combination of Eqs.(1) and (2.b) gives Helmholtz equation (assume constant density)

$$\frac{d^2P}{dz^2} + k^2 P = 0, k = \frac{\omega}{v_r \sqrt{Y}} \quad (3)$$

To achieve a complex damping function we can follow Horton (1959) and introduce the notation

$$Y(\omega, \tau) = A(\omega, \tau) + iB(\omega, \tau) \quad (4)$$

In his paper, Horton gives examples of values of A and B for various absorption models that can be causal or non-causal. Since the wavenumber k is in focus, the following expression is now elaborated on

$$\frac{1}{\sqrt{Y}} = \frac{1}{\sqrt{A+iB}} = \frac{\sqrt{A-iB}}{\sqrt{A^2+B^2}} = \frac{(A^2+B^2)^{1/4} [\cos(u/2) - i \sin(u/2)]}{(A^2+B^2)^{1/2}} = \frac{[\cos(u/2) - i \sin(u/2)]}{(A^2+B^2)^{1/4}}$$

$$\tan(u) = \frac{B}{A} \quad (5)$$

Moreover, the following trigonometric relations are valid

$$\tan(u) = \frac{\sin(u)}{\cos(u)} = \frac{\sin(u)}{\sqrt{1-\sin^2(u)}} = \frac{\sqrt{1-\cos^2(u)}}{\cos(u)} = \frac{B}{A} \Rightarrow \quad (6)$$

$$\cos(u) = \frac{A}{\sqrt{A^2+B^2}}, \quad \sin(u) = \frac{B}{\sqrt{A^2+B^2}}$$

And also these

$$\cos(u/2) = \sqrt{\frac{1+\cos(u)}{2}}, \quad \sin(u/2) = \sqrt{\frac{1-\cos(u)}{2}} \quad (7)$$

Finally, combination of Eqs. (5)-(7) gives the result

$$k = \frac{\omega}{v_r \sqrt{Y}} = \frac{\omega}{v_r \sqrt{A+iB}} = \frac{\omega}{v_r} \left[\frac{1}{\sqrt{A}} - \frac{i}{2} \frac{B}{A\sqrt{A}} \right] \quad (8)$$

Now we will compare the real and imaginary part of k for the Q-models. The real part can be related to the phase velocity and the imaginary part is the attenuation coefficient. Then we have: $k_{real} = \frac{\omega}{v_r} \frac{1}{\sqrt{A}}$

$$\text{and } k_{imag} = \frac{1}{2} \frac{\omega}{v_r} \frac{B}{A\sqrt{A}} \quad (9)$$

This leads up to different functions A and B that was calculated in Sørdsal (2019) and can be related to Q-models. The outline is also given in appendix 1 and is listed in table 1.

		A	B
1	Kolsky - Wang	$\left[\frac{\omega}{\omega_h} \right]^{2\gamma} \gamma = \frac{1}{\pi Q}$	$\left[\frac{\omega}{\omega_h} \right]^{2\gamma} \frac{1}{Q}$

Table 1. Forward Q-filter

Fig.6. shows \sqrt{A} (which gives us a hint about the dispersion) for Kolsky-Wang. (Multiplying \sqrt{A} with the reference velocity v_r gives us the phase velocity). According to Kolsky, the tuning frequency ω_h should be the smallest frequency in the frequency band and. Wang modified the Kolsky model by choosing the highest frequency in the frequency band. And that will be the Nyquist frequency $2\pi\omega_h = 125$ Hz (blue graph on fig.6.)

For the attenuation coefficient Fig.2. we used $Q=100$ (blue graph) and $Q=50$ (green graph). The attenuation coefficient increase linear with frequency. An important aspect with the Kolsky model is that the attenuation will be strictly linear with frequency over the range of measurement.

From fig.6. we can readily see that more damping (red graph) gives the lower graph. This means that the less damping, the faster will go the reflectors. We will see this when we compute the synthetics.

Attenuation coefficient

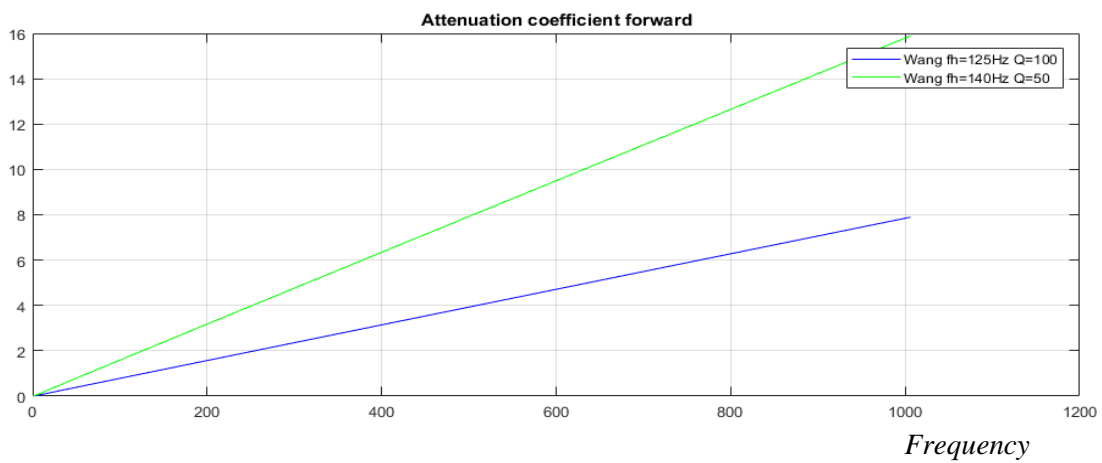


Fig.5. Attenuation coefficient. Attenuation coefficient is dimensioned pr. km or pr.sec.

Phase velocity

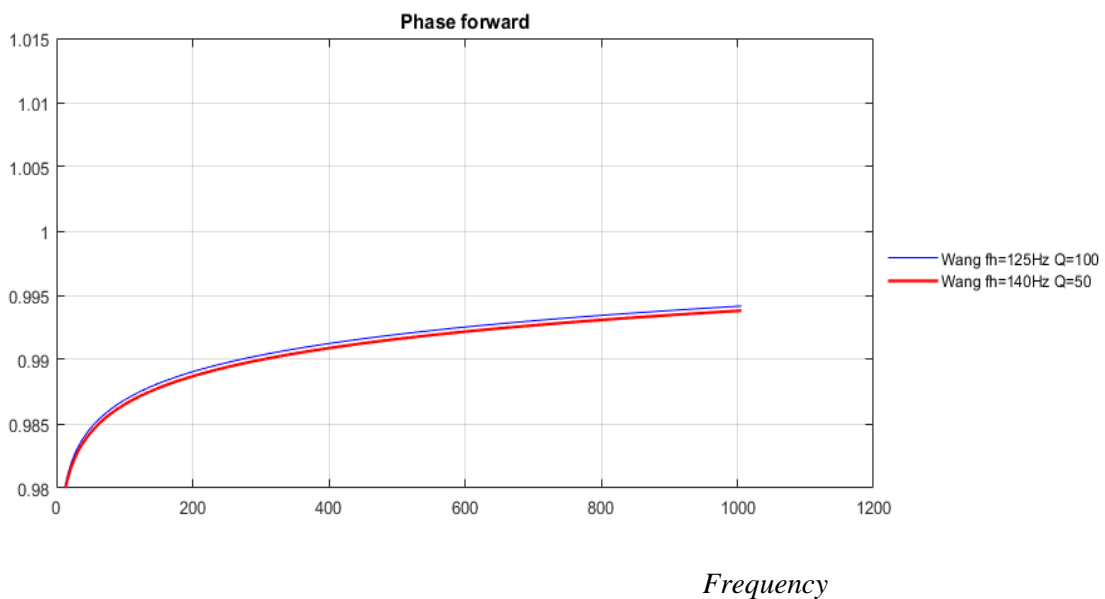


Fig.6. Phase velocity for forward Q-model of table 1. We have used $Q=50$. Wang fh=140Hz (red) Wang fh=125Hz (red) ($\omega_h=2\pi f_h$), $Q=100$. Phase velocity is dimensionless.

Introducing the Riccati equation with absorption

The basic idea in a downward wave propagation migration approach is that the wavefield at the surface of the seismic earth model is extrapolated down to a depth z . The real part of k in Eq. (9) describes all dispersion effects during wave propagation and the imaginary part describes absorption.

From Nilsen and Gjevik (1978) we have the Riccati equation:

$$\frac{dK}{dz} = \frac{2i\omega}{v_r \sqrt{Y}} K - r(1 - K^2) \quad (10)$$

K is the complex reflection coefficient and r is the depth-dependent ‘reflectivity’ per depth unity:

$$r(\tau) = \frac{1}{2\rho v_r} \frac{d(\rho v_r)}{d\tau} \quad (11)$$

Since vertically travelling waves are considered, the transformation from depth to two-way traveltime is straightforward

$$\tau = 2 \int_0^z \frac{dz}{v_r}, \Rightarrow d\tau = \frac{2}{v_r} dz \quad (12)$$

Which gives the travel time version of Eq.(10)

$$\frac{dK(\omega, \tau)}{d\tau} = \frac{i\omega}{\sqrt{Y(\omega, \tau)}} K(\omega, \tau) - r(\tau)(1 - K^2), r(\tau) = \frac{1}{2\rho v_r} \frac{d(\rho v_r)}{d\tau} \quad (13)$$

By noticing that

$\exp(-i\omega \int_0^\tau Y(\omega, \tau))^{-1/2} d\tau \equiv \exp[-\phi(\omega, \tau)]$ is an integrating factor for this Riccati equation, it can

be rewritten on the following form:

$$\frac{d}{d\tau} [K(\omega, \tau) \exp(-\phi(\omega, \tau))] = -r(\tau)(1 - K^2) \exp(-\phi(\omega, \tau)) \quad (14)$$

$$\text{Where } \phi(\omega, \tau) = i\omega \int_0^\tau \frac{d\tau}{\sqrt{Y(\omega, \tau)}} = i\omega \int_0^\tau \left[\frac{1}{\sqrt{A}} - \frac{iB}{2A\sqrt{A}} \right] d\tau = \int_0^\tau \left[\frac{i\omega}{\sqrt{A}} + \frac{\omega B}{2A\sqrt{A}} \right] d\tau \quad (15)$$

Assume now the following boundary condition: $K=0$ when $\tau \geq T$. Integration of Eq. (14) now gives the solution

$$-K(\omega, \tau) \exp(-\phi(\omega, \tau)) = - \int_\tau^T r(\tau') \exp(-\phi(\omega, \tau')) (1 - K^2(\omega, \tau')) d\tau' \quad (16)$$

From Eq.(16) we can, when $K^2 \ll 0$, obtain the non-linear solution

$$K(\omega, \tau) = \exp(\phi(\omega, \tau)) \int_\tau^T r(\tau') \exp(-\phi(\omega, \tau')) (1 - K^2(\omega, \tau')) d\tau' \quad (17)$$

Equation (17) is now the starting point for a non-linear modelling algorithm. Assume a discretization in τ (sample interval $\Delta\tau$ and total of N points), and then start at maximum time $T=(N-1) \Delta\tau$ and then calculate K in upward direction.

We introduce the following notation for convenience

$$\begin{aligned} K_{i,j}^n &= K^n(\omega_i, \tau_j) \quad \tau_j = (j-1)\Delta\tau, j = N-1, N-2, \dots, 1 \\ K_{i,N}^n &= 0 \end{aligned} \quad (18)$$

Where the superscript n implies iteration number.

Next, define (trapezoidal rule applied to integral in Eq.(17)) (assume (n+1) th. iteration)

$$\begin{aligned} \beta_{i,j} &= \frac{\Delta\tau}{2} \left[r_{j+1} X_{i,j+1} \left\{ 1 - (K_{i,j+1}^n)^2 \right\} + r_j X_{i,j} \left\{ 1 - (K_{i,j}^n)^2 \right\} \right], j = N-1, N-2, \dots, 1 \\ r_N &= 0 \end{aligned} \quad (19)$$

Which gives the after sought solution

$$K_{i,j}^{n+1} = \beta_{i,j} / X_{i,j}, j = N-1, N-2, \dots, 1 \quad (20)$$

In Eqs.(18 and 19) we have introduced the operator

$$X_{i,j} = \exp[-\phi(\omega_i, \tau_j)] \tau_j = (j-1)\Delta\tau \quad (21)$$

The seismogram corresponds to the solution $j=1$. The final result in time is obtained after an inverse FFT.

Let the first layer be water, then we need to include the free-surface multiples. Assume that τ_ω represents two-way vertical travel time in the water layer. Total field P_i recorded at the surface (e.g. including multiples) can then be written as (r being the reflection coefficient of the seafloor)

$$P_i = K_{i,j=1} \left[1 - r \exp(-i\omega_i \tau_\omega) + r^2 \exp(-2i\omega_i \tau_\omega) + \dots = \frac{K_{i,j=1}}{1 + r \exp(-i\omega_i \tau_\omega)} \right] \quad (22)$$

Forward numerical implementation

When we make calculations with the models we need to define $r(\tau)$ from a set of layered model parameters connected to the impedance of a seismic media. We can, of course, get r_j from eq (22) as reflectivity per depth unit (1/s). Invoking Eq.(23) we can calculate two-way traveltimes by converting the layer thickness z into time and using:

$$r(\tau) = \frac{1}{2(\tau_{j+1} - \tau_j)} \left[\frac{\rho_{j+1} V_{j+1}}{\rho_j V_j} - 1 \right] \quad j=1, \dots, NT-1 \quad (23)$$

We can then get R_j (Reflection coefficients) either by setting ρ and v direct into Eq.(24) or setting r from Eq (23) into Eq.(24). Both r and R are similar physical parameters which represents the contrast in acoustic impedance across an interface. To proceed with computations we must discretize every layer in the model with j and move down to the layer $NT-1$. Velocity and density for each layer we find in table 3.

(24)

$$R_j = \frac{\rho_{j+1} v_{j+1} - \rho_j v_j}{\rho_{j+1} v_{j+1} + \rho_j v_j} = \frac{\exp[2\Delta\tau r_{j+1}] - 1}{\exp[2\Delta\tau r_{j+1}] + 1} \text{ for } j = 0, 1, 2, \dots, NT - 1$$

To set up table 3 for our model parameters we need some data from the Sleipner field for different CO2-saturations. These data we achieved from Nordahl (2015).. The CO2-saturation is important when we study the CO2-plume. Data are in table 2. Studying fig.4, we were able to set up a model roughly with CO2-layers 25 m thick and from fig.7 we could locate maximum saturation and put Q-data into table 3. Figure 7 gave us an idea of absorption as a function of CO2 saturation.

CO2-saturation	R (reflection coefficient)	P-velocity (m/s)	Density(kg/m3)
0 %		2048	2047
10 %	-0,0821	1672	2039
20 %	-0,1175	1568 (1563)	2031
30 %	-0,1363	1511	2022 (2030)
40 %	-0,1476	1482	2014
50 %	-0,1555	1470 (1464)	2006
60 %	-0,1619	1451	1998
70 %	-0,1664	1443	1990
80 %	-0,1705	1437	1982
90 %	-0,1738	1433	1974
100 %	-0,1769	1437	1965 (1966)

Table 2.a. parameters from Nordahl (2015).

The background model gives us the structure of the sediments without CO2. Different saturations with CO2 will give us different values for velocity and density. This is deviation from the background model. Numbers for the background model can be found in Table 2.b. Also absorption will change for different saturations in table 3. I have given alternative values from background model in yellow color on table 3.

It is important to realize that we consider numbers that are taken from Table 2.a and Table 2.b and roughly estimated from the available numbers. Other numbers will be introduced in other articles in the future. Q-values are estimated from fig.7, but also estimated from values that were usable in the seismic theory.

Layer	P-Velocity (m/s)	Density (kg/m ³)
Water layer (0-80m)	1480	1000
Upper unit (80-720m)	2000-2180	1850-2017
Pliocene Shale (bedrock) (720-820)	2180-2360	2017-2183
Utsira sand (820-1030)	1950-2100	1960-2080
Lower unit (1030-2000)	2200-2500	2035-2313

Table 2.b. parameters from Nordahl (2015).

Fig.7 shows us that CO₂-saturation between 5-10% give highest absorption (and lowest Q-values). Therefore we will choose lowest Q-values in most saturated layers (grey colored on Table 3). Fig.7. gives Q about 100 when saturation is near 50 %. However, we will choose less damping to avoid problems with the calculations.

Q	Depth) Layers	Density ρ g/cm ³	Bgr. dens.	Velocity v km/h	Backgr. velocity	Saturation CO ₂	Depth	Layers
Q1=200	80	1.0	1.0	V1=1480	1480	0 %	80	Water layer
Q2=200 100	560	1.5	1.5	V2=1600	1600	45 %	640	Layer 2
Q3=200 100	80	2.0	2.0	V3=2000	2000	45 %	720	Layer 3
Q4=200 100	155	2.03	2.0	V4=1800	1800	45 %	875	Layer 4
Q5=200 100	25	1.965 2.006	1.966	V5=1437	1470	100%	900	Layer 5
Q6=200 100	25	1.965 2.006	1.5	V6=1437	1500	100%	925	Layer 6
Q7=200	25	2.006 2.03	1.966	V7=1470	1430	50 %	950	Layer 7
Q8=200	25	2.03	1.5	V8=1568	1600	25 %	975	Layer 8
Q9=200	25	1.965	1.966	V9=1430	1430	25 %	1000	Layer 9
Q10=200	25	1.5	1.5	V10=1568	1600	25 %	1025	Layer 10
Q11=200	25	1.96	1.966	V11=2500	2500	25 %	1050	Layer 11

Table 3. Seismic model parameters large model

We choose 2500 m/s for Layer 11, background model that is consistent with Table 2.b. Layer 1 (water layer) is also consistent with Table 2.b. Values for other parameters, however, are chosen in a way that

made calculations possible. It will be a challenge for future research to find better agreement between Table 3 and measurements from Table 2.a. and b. and Q-values from fig. 7. I will mention that the choice of Q-values and CO2 saturation for layer 1 to layer 3 is for practical computations. For real data one could suspect no CO2-saturation above layer 4, and therefore not lower absorption. This is the case if layer 4 is the caprock.

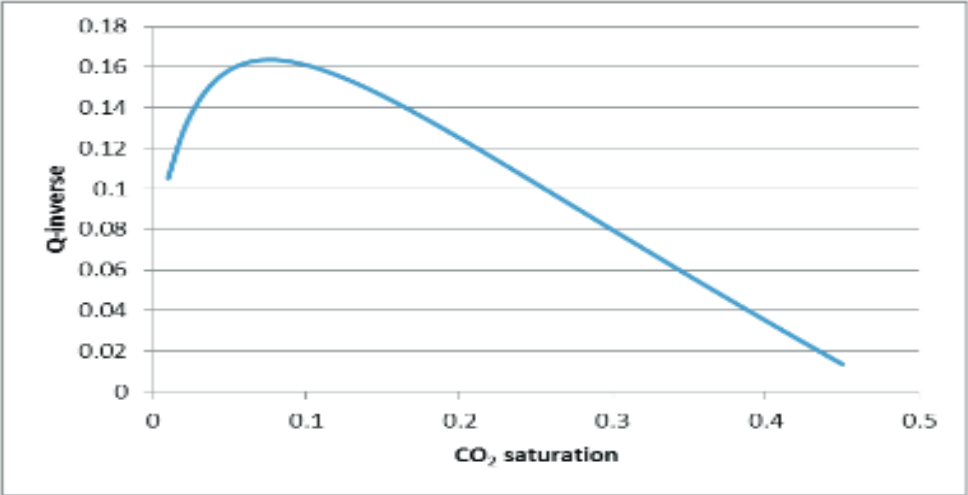


Fig.7 Q-values for CO2 saturation

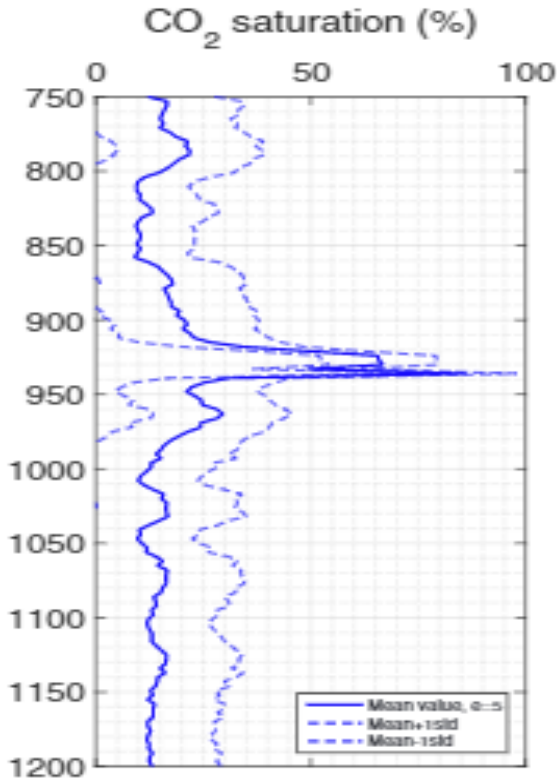


Figure 8. 1D profiles of CO2-saturation estimation taken from Hong Yan (2018). The data is from Utsira sand, Sleipner field. Vertical axes is depth in meters. The CO2-saturation is maximum (estimated 100%) between 900 and 950 meters (marked in table 3).

Values for CO2 in Table 3 are based on roughly estimates from fig.7 and. fig.8. Different saturations with CO2 will give us different parameters for Table 3. Saturation is maximum for depth between 900 and 950 meters and this is marked with grey on Table 3.

Maximum absorption is around 8 % saturation, but Table 3 starts with 0% CO2 saturation in the water layer. Fig.5 also shows that CO2-saturation around 45% will give absorption ($1/Q=0,02$). As mentioned above what is important is to find values that were usable in the seismic theory, and we had to try different parameters to get good results, especially for the inversion.

I used some of the data from table 3 for the synthetics Eq.(17). The tables are an attempt to include more accurate data for the section taking also the CO2-saturation into account. The free-surface-multiples were easily introduced and required a water layer (80m depth) above the other layers as introduced in Eq.(22). Density of the water layer is 1 g/cm3 and velocity is 1480 km/h. The synthetics with free-surface multiples are graphs on fig.9 from left.

With a background model without attenuation we achieved the synthetics with surface-multiples as the black trace on the left fig.9. Red graph in same plot is synthetics with interbed and free-surface-multiples absorption included. Then we have cplot with both interbed and free-surface multiples. Free-surface multiples are dominant compared to interbeds. The reflectors are then introduced to the right for the cplot (black). For attenuation we used $Q1=Q2=Q3=100$. We have used the absorption model of Wang with $2\pi\omega_h=140$ Hz. Reflectors are easily visible on all plots (red circles for the first 4 reflectors).

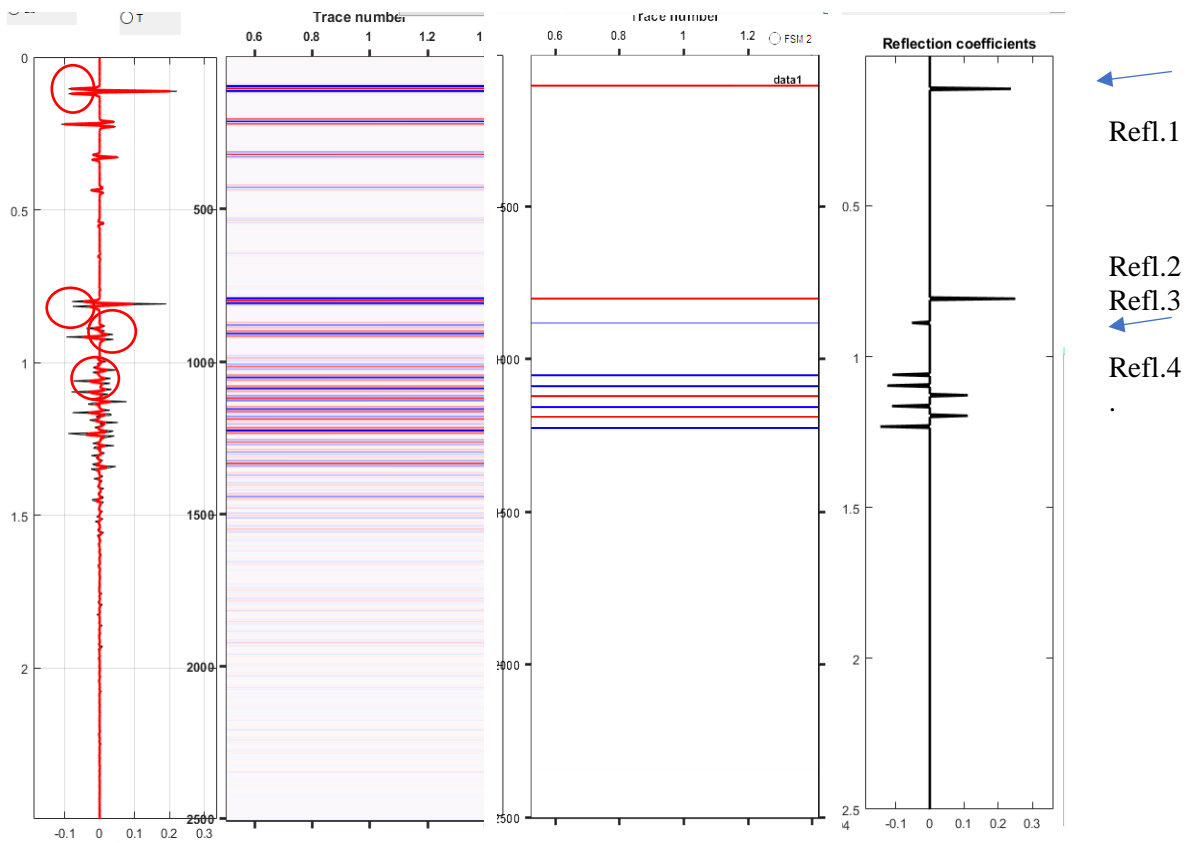


Fig. 9. We used $Q1=Q2=Q3=100$. We have used the absorption model of Wang with $\omega_h=2\pi 140$ Hz. The next plot to the right shows synthetics without attenuation (black) and with attenuation (red). Then to the right we have synthetics with free surface-multiples and with interbed multiples. Then comes c-plot without any multiples. To the right we have reflection coefficients.

Then we have cplot for the background model. Here we have no multiples and no absorption so this is simply a reflection coefficient series for the background model. An inversion of the synthetics in fig.9 should give us this very solution.

Before we jump to the inversion, we need to give a remark about the impedance. The relation between r and the impedance makes it possible to compute the impedance for every solution of r . If the acoustic impedance I_0 is known at $z = 0$, (or at any depth), I is also uniquely determined as a function of τ . From Eq. (11) we can deduce:

$$I = I_0 \exp\left(2 \int_0^\tau r(\tau) d\tau\right) \quad (25)$$

where $I_0 = \rho_0 v_0$ and I/I_0 will give us a dimensionless relative impedance. We will come back to this in the next section.

Inversion LSQ – inverse numerical implementation

In the following we will implement the layered model parameters (Table 3) that was used to generate the synthetic seismograms in the forward modeling above. The inversion will be done taking the forward modelled synthetic seismograms as input. The procedure will be done with a conventional least square (LSQ) seismic inversion procedure. We will see that an LSQ-inversion is all we need to recover the reflection coefficients from the synthetics .

Consider Eq. (17) in the limit $\tau \rightarrow 0$, which gives the ‘seismogram’

$$K(\omega, 0) = \int_0^T r(\tau') \exp(-\phi(\omega, \tau')) (1 - K^2(\omega, \tau')) d\tau' \quad (26)$$

Introduce ‘reflectivity’ series

$$r(\tau) = \Delta \tau \sum_{i=0}^{NT-1} r_i \delta(\tau - i\Delta \tau), T = NT \cdot \Delta \tau \quad (27)$$

Combination of Eqs. (26) and (27) gives

$$K(\omega, 0) = \sum_{i=0}^{NT-1} r_i \exp(-\phi(\omega, i\Delta \tau)) (1 - K^2(\omega, i\Delta \tau)) \Delta \tau \quad (28)$$

Originally, seismogram recorded in timedomain, i.e. $k(t, 0)$, and assume sampled with a total of NT -samples. Fourier transform of the data will give the same number of monochromatic seismograms.

Nilsen and Gjevik introduced an iterative inversion procedure to solve for r in eq.(26) when the reflection response of the reflecting layer is known. When absorption was included that could be a complicated process and as far as we know no calculations were done with absorption by them.

Leiv Gelius, in an unpublished note, suggested a more elegant solution of the equation with the matrix system:

$$\begin{bmatrix} K_{n+1}(\omega_0, 0) \\ K_{n+1}(\omega_1, 0) \\ \vdots \\ K_{n+1}(\omega_{NT-1}, 0) \end{bmatrix} = \quad (29)$$

$$\begin{pmatrix} \exp(-\varphi(\omega_0, 0)(1 - K_{0,n}^2)) & \exp(-\varphi(\omega_0, \Delta\tau)(1 - K_{1,n}^2)) & \dots & \exp(-\varphi(\omega_0, (NT-1)\Delta\tau)(1 - K_{n,n}^2)) \\ \exp(-\varphi(\omega_1, 0)(1 - K_{0,n}^2)) & \exp(-\varphi(\omega_1, \Delta\tau)(1 - K_{1,n}^2)) & \dots & \exp(-\varphi(\omega_1, (NT-1)\Delta\tau)(1 - K_{n,n}^2)) \\ \vdots & \vdots & \dots & \vdots \\ \exp(-\varphi(\omega_{NT-1}, 0)(1 - K_{0,n}^2)) & \exp(-\varphi(\omega_{NT-1}, \Delta\tau)(1 - K_{1,n}^2)) & \dots & \exp(-\varphi(\omega_{NT-1}, (NT-1)\Delta\tau)(1 - K_{n,n}^2)) \end{pmatrix} \begin{pmatrix} r_{n,0} \\ r_{n,1} \\ \vdots \\ r_{n,NT-1} \end{pmatrix}$$

Hagos (2016) made some computations for Eq.(29) in his thesis. A more detailed study of the solution is in appendix 2. The mathematics for how to do least square inversion is also outlined in Sørdsal (2018).

Note that $K_0^2=0$ in the first iteration. After a new estimate of the reflectivity series has been obtained, an update of $K_{i,n}^2$ can be obtained by solving the forward problem. Iterations are carried out until the relative change in reflectivity is below a certain user threshold. The effect of the inversion when $K^2 = 0$ is simply to compensate for the damping of the amplitude caused by attenuation and correct the phase term caused by dispersion. When $K^2 \neq 0$ we also remove multiples and compensate transmission loss. Surface multiples can also be removed simply by multiplying K with the inverse of RHS of Eq (22). First we remove surface multiples before we solve Eq.(29). This can simply be done multiplying r with the inverse of Eq. (22). Fig.10 shows both the synthetics (Eq.17) and the inversion Eq.(29) with the synthetics r as input. I took the first plot (red) from left on fig.9 as input. The inversion (middle plot) gives us a sharp layer (blue). Right plot from middle plot shows the impedance and then the reflector model. When we change velocity V_3 from 2400 till 2000, we achieve the change that can be seen on the impedance. The inversion will not correct change due to change in velocity.

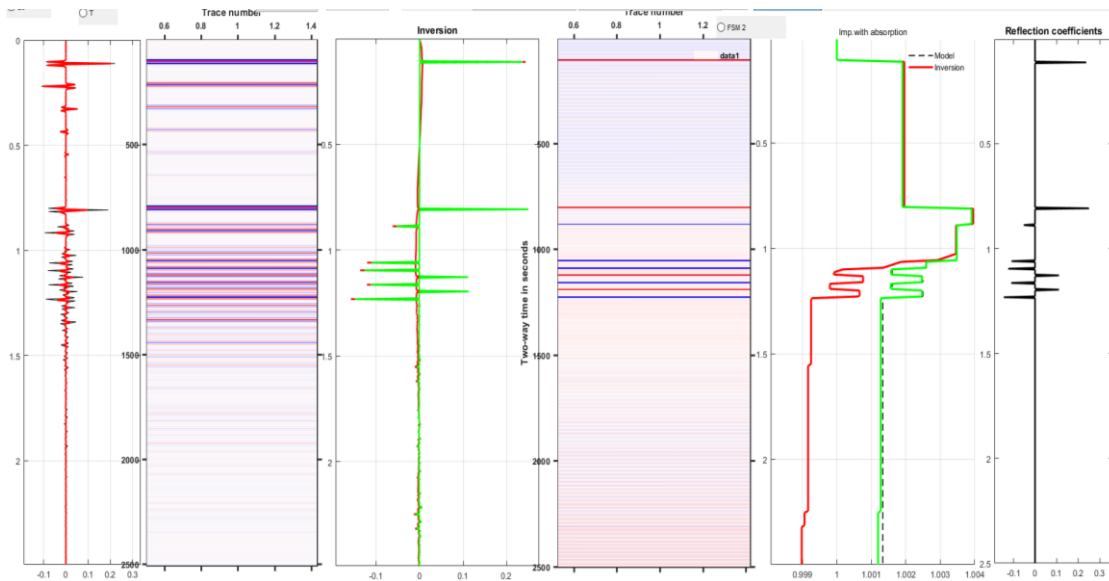


Fig.10. Data from Table 3. green : $V_3=2400, Q_3=100$, Parameters are changed to red: $Q_3=100, V_3=2000$ m/s. Only velocity is changed.

Fig.9-10 shows calculations with data from the first 3 reflectors. Will we get more problems using more reflectors?

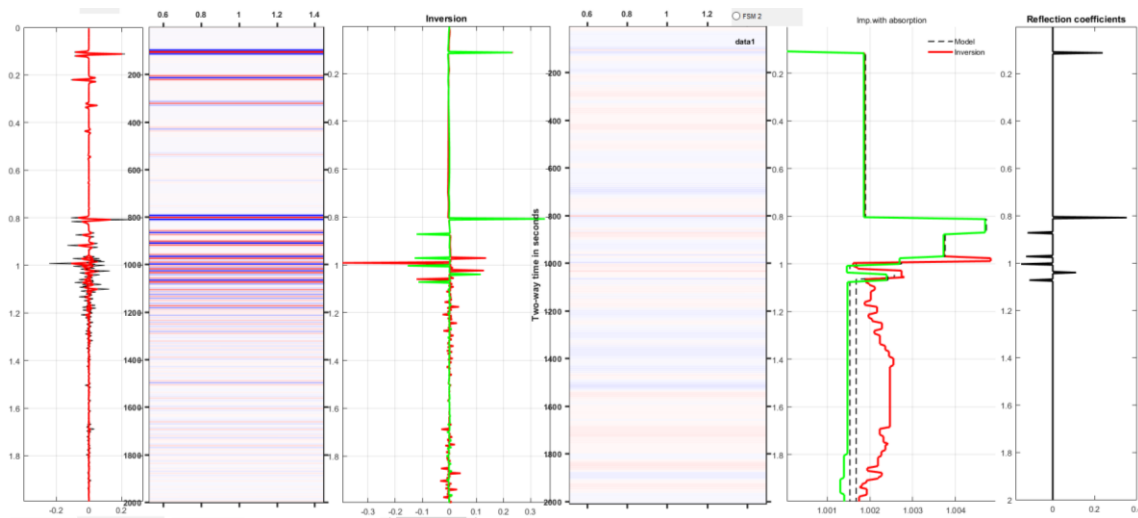


Fig.11. Green: $V_5=1500$ red: $v_5=2500$

On fig.11. we have changed velocity V_5 . From 1500 to 2500. We can see a change in the impedance. We could expect that the impedance inversions could show a solution very different from the background model, and we can expect problems studying inversion with high attenuation. But I will concentrate on small deviation from the background model, and only consider change in velocity.

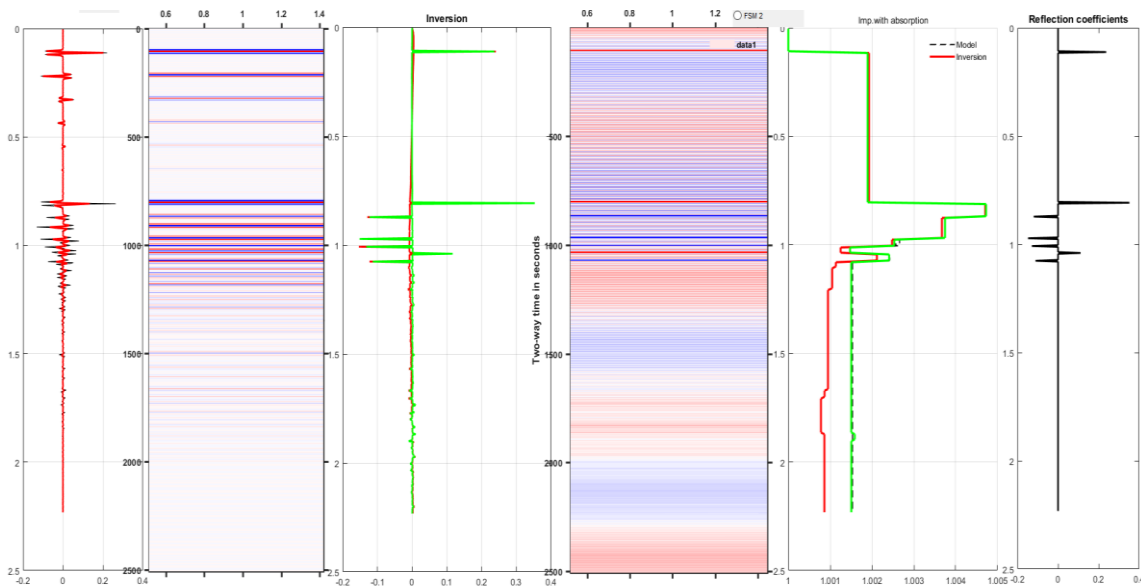


Fig.12. Red=1470, green=1437

Fig.12 shows calculations that has no change in absorption. However the velocity V_5 is changed from 1470 (background model green) to 1437 (red saturated model.) We can see a smaller change in impedance than on fig.11 (that has smaller velocity-change). However some noise is introduced on the plot of the inversion.

A closer look at the inversion

Ultimately, after the development of the previous theory we have been able to combine a forward solution of Kolsky-Wang Q-filter with a LSQ-solution for inversion. So we have fulfilled the purpose

of this article. However, a broader view of the subject could be interesting in the future and a further study of Q-filtering is necessary as well as more studies of velocity change.

So, to even further sum up: setting $K^2=0$ in eq (29) we achieved the linear solution on matrix form and solved this for r as a time-domain vector that represents the filter. The inverse Q-filtering procedure was performed successively to each time sample to get the time-dominant output vector. We then used the output r as input getting the inverted solution for a new inverted r . When we do this we can, of course, replace the Q-filters with the inverse Q-filters as Wang did, and this could be a further study. Then we also will need to study the stabilization of the inverse filter, gain limitation and so on. However, the LSQ-solution in this paper simplified the study. A more complicated theory for the LSQ-solution are introduced in appendix 2. It is called the regularization of the LSQ-solution. It was not necessary to introduce regularization in this study, to achieve the goal of the paper, but could be a subject for further study.

Further iterations in the Riccati-solution introduced non-linearity on the way to a seismic theory that can be used on real data and will be, as far as I can see, a broader and better theory than the theory of Wang that was strictly linear. And, of course, the application of the theory applied on CO₂-monitoring is more relevant in today's world than traditional seismic for oil prospecting. I have also shown that CO₂ in the seismic structure will introduce some problems that will be complicated to solve. Velocity changes in the CO₂-saturated structure compared to the background model will introduce problems in addition to problems caused by absorption.

Conclusion

The results of the preceding sections show that the Riccati equation with Q-filtering provides a method for the construction of synthetic reflection seismograms that is a continuation of the method introduced by Nilsen and Gjevik. Moreover does this theory describe a method for inverting reflection data, i.e. computing the variations in the acoustic impedance within a reflecting layer that can be used in real prospecting. This I have briefly suggested by introducing a water layer over a very simple seismic model and a more complicated seismic model from the Sleipner field. And the Riccati inversion corrects phase, compensates frequency loss, removes multiples and compensates transmission loss in one single process.

In my previous articles I tested the abilities of the inversion method by inverting a synthetic reflection seismograms computed from a simple impedance model with a water layer. And frankly, this article does not introduce so much more that concern real seismic prospecting. It would, however – as Gjevik suggested several years ago - be interesting to apply the present inversion method to real reflection data from a more complex structure. A number of problems will then arise as was discussed in the paper of Nilsen and Gjevik. However, because of years of rapid development in inversion theory, this is much easier solved today than when the theory first was introduced.

Even if this could be done only with a limited degree of accuracy, the main problem is, however, that what Gjevik asked is not fully answered: will one lose so much information or introduce so many errors through this process that the inversion becomes meaningless when applied to real prospecting? In view of the success of the application on data from the Sleipner field this question could soon be answered.

References

- Gjevik et al. (1976) An attempt at the inversion of reflection data. Geophysical prospecting 24,492-505*
Nilsen and Gjevik (1978): Inversion of reflection data. Geophysical prospecting 26, 421-432
Yanguhua Wang (2008) Blackwell Publishing. Seismic inverse Q filtering

Knut Sørdsal (1981) Viskoelastiske dempningsmodeller i Riccatiligningen anvendt i marin seismikk. University of Oslo

Knut Sørdsal (2019) Seismic Q-filter models applied to the Riccati equation
https://www.researchgate.net/publication/337682839_Seismic_Q-filter_models_applied_to_the_Riccati_equation

Knut Sørdsal (2018) 1-D non-linear inversion of data with absorption - revisited.
https://www.researchgate.net/publication/331257025_1-D_non-linear_inversion_of_data_with_absorption_-_revisited

Bland(1960) The theory of linear viscoelasticity. Pergamon Press

Horton (1959) A loss mechanism for the Pierre Shale. Geophysics vol.24, no 4

Aki and Richards (2002) Quantitative Seismology W.H. Freeman and Co. San Fransisco

Kolsky, 1956 The propagation of stress pulses in viscoelastic solids. Philosophical Magazine 1, 693-710

Kjartansson E. 1979 Constant Q wave propagation and attenuation. Journal of Geophysical Research 84 4737-48.

Futterman W.I 1962 Dispersive body waves. Journal of Geophysical Research 67 , 5279-91

Trorey A.W, 1962 Theoretical seismograms with frequency and depth dependent absorption. Geophysics 27, 766-85

Claerbout J.F.1976 Fundamentals of Geophysical Data Processing. McGraw-Hill Book Co. New York

Hagos Geberehiwet Gebregergs (2016): Compensation of Absorption Effects in Seismic Data. University of Oslo

Hong Yan, Bastien Dupuy, Anouar Romdhane and Børge Arntsen
Geophysical Prospecting, 2019, 67, 1055–1071 CO₂ saturation estimates at Sleipner (North Sea) from seismic tomography and rock physics inversion

Janita Louise Nordahl : (2015) Modeling of seismic amplitude anomalies associated with CO₂ underground storage — EOM-3901 Master's Thesis in Energy, Climate and Environment

KARSTENS, J. & BERNDT, C. 2015. Seismic chimneys in the Southern Viking Graben – Implications for palaeo fluid migration and overpressure evolution. Earth and Planetary Science Letters, 412, 88-100.

HALLAND, E. K., JOHANSEN, W. T. & RIIS, F. 2011. CO₂ Storage Atlas Norwegian North Sea, Norwegian Petroleum Directorate.

ARTS, R., EIKEN, O., CHADWICK, A., ZWEIGEL, P., VAN DER MEER, B. & KIRBY, G. 2004a. Seismic monitoring at the Sleipner underground CO₂ storage site (North Sea). Geological Society, London, Special Publications, 233, 181-191.

ARTS, R., EIKEN, O., CHADWICK, A., ZWEIGEL, P., VAN DER MEER, L. & ZINSZNER, B. 2004b. Monitoring of CO₂ injected at Sleipner using time-lapse seismic data. Energy, 29, 1383-1392.

Hiroyuki Azuma (2014) Utilization of seismic attenuation in the monitoring of CO₂ geological storage project. Science Direct.

Appendix 1

In the literature the wavenumber k is often written on the following form in case of absorption (constant- Q model)

$$k = \frac{\omega}{v(\omega)} \left[1 - \frac{i}{2Q} \right] = \frac{\omega}{v_r} + \left[\frac{\omega}{v(\omega)} - \frac{\omega}{v_r} \right] - i\alpha(\omega) = \frac{\omega}{v_r} + \varphi(\omega) - i\alpha(\omega). \quad \alpha = \frac{\omega}{2Qv(\omega)} \quad (\text{A.1})$$

Where α is the absorption coefficient and φ is the phase of the ‘absorption filter’. In order to ensure causality, the filter should be minimum phase. For such a filter this relationship holds.

$$\varphi(\omega) = \text{H} [\alpha(\omega)]$$

With H denoting the Hilbert Transform. In case of no dispersion ($\varphi=0$), the filter will be noncausal. Then we have

$$k = \frac{\omega}{v_r \sqrt{Y}} = \frac{\omega}{v_r \sqrt{A + iB}} = \frac{\omega}{v_r} \left[\frac{1}{\sqrt{A}} - \frac{i}{2} \frac{B}{A\sqrt{A}} \right] \quad (\text{A.2})$$

Equating Eqs. (A.1) and (A.2) gives the relationships

$$A = \left[\frac{v(\omega)}{v_r} \right]^2 \quad B = \left[\frac{v(\omega)}{v_r} \right]^2 \frac{1}{Q}, \quad (\text{A.3})$$

Aki and Richards (2002) show that the following relation should be held to honor causality

$$\frac{\omega}{v(\omega)} - \frac{\omega}{v_\infty} = \text{H} \left[\frac{\omega}{2Qv_\infty} \right] \quad (\text{A.4})$$

Where v_∞ is the limit of the velocity function when ω tends to infinity. Equation (12) can be further approximated as

$$\frac{\omega}{v(\omega)} - \frac{\omega}{v_h} \cong \text{H} \left[\frac{\omega}{2Qv_\infty} \right] \quad (\text{A.5})$$

Where v_h is the velocity related to the highest possible (tuning) frequency of the seismic band. The wavenumber is accordingly adjusted as (compare with Eq.(A.1)).

$$k = \frac{\omega}{v_h} + \left[\frac{\omega}{v(\omega)} - \frac{\omega}{v_h} \right] - i \frac{\omega}{2Qv(\omega)} = \frac{\omega}{v_h} \left\{ 1 + \left[\frac{v_h}{v(\omega)} - 1 \right] - i \frac{v_h}{2Qv(\omega)} \right\} \quad (\text{A.6})$$

And combined with a Kolsky type of phase-velocity model (Kolsky, 1956)

$$v(\omega) = v_h \left(\frac{\omega}{\omega_h} \right)^\gamma, \quad \gamma = (\pi Q)^{-1} \quad (\text{A.7})$$

Gives the wavenumber model

$$k = \frac{\omega}{v_h} \left[1 + \left[\left(\frac{\omega}{\omega_h} \right)^{-\gamma} - 1 \right] - \frac{i}{2Q} \left(\frac{\omega}{\omega_h} \right)^{-\gamma} \right] \quad (\text{A.8})$$

Which has been employed by Wang. From Eqs. (A.1) and (A.2) it also follows that ($v_r=v_h$)

$$A_{Wang} = \left[\frac{\omega}{\omega_h} \right]^{2\gamma} B_{Wang} = \left[\frac{\omega}{\omega_h} \right]^{2\gamma} \frac{1}{Q} \quad (\text{A.9})$$

From Eq.(A.9) it follows that $0 < A_{Wang} < 1$, and the same for B_{Wang} but with $B_{Wang} \ll A_{Wang}$.

Based on Eq. (A.3), Kjartansson (1979) proposed an alternative wavenumber model

$$k = \frac{\omega}{v_\infty} + \left[\frac{\omega}{v(\omega)} - \frac{\omega}{v_\infty} \right] - i \frac{\omega}{2Qv_\infty} = \frac{\omega}{v_\infty} + H \left[\frac{\omega}{2Qv_\infty} \right] - i \frac{\omega}{2Qv_\infty} \quad (\text{A.10})$$

From Eqs.(11) and (A.10) it follows that ($v_r=v_\infty$)

$$A_{Futt} = \left[1 + \frac{1}{\omega} H \left(\frac{\omega}{2Q} \right) \right]^{-2} B_{Futt} = (A_{Futt})^{3/2} \frac{1}{Q} \quad (\text{A.11})$$

For completeness, we also have the dispersion-free and non-causal absorption model of Futterman (1962), which corresponds to

$$A_{Futt} = 1 \quad B_{Futt} = \frac{1}{Q} \quad (\text{A.12})$$

Ricker wavelet in the synthetics

In order to get the synthetic seismogram in time domain by inverse Fourier transform of the complex reflection coefficient K, each component of K (Eq.(26) is multiplied by a sampled Ricker wavelet in frequency domain:

$$Srw = (2/(\sqrt{\pi})) \frac{f^2}{f_c^3} \exp\left(-\frac{f}{f_c}\right)^2 \quad (\text{A.13})$$

This Ricker wavelet is a zero-phase wavelet and is non-causal. The frequency f_c is called the center frequency and will vary.

Appendix 2

To apply least-square inversion, Eq. (29) can be written in vector and matrix notation in short as

$$\vec{K} = M \vec{r} \quad (\text{A14})$$

where

$$\vec{K} = \begin{bmatrix} K_{n+1}(\omega_0, 0) \\ K_{n+1}(\omega_1, 0) \\ \vdots \\ K_{n+1}(\omega_{NT-1}, 0) \end{bmatrix} \quad \vec{r} = \begin{bmatrix} r_{n,0} \\ r_{n,1} \\ \vdots \\ r_{n,NT-1} \end{bmatrix}$$

$$M = \Delta\tau \begin{pmatrix} \exp(-\varphi(\omega_0, 0)(1-K_{0,n}^2)) & \exp(-\varphi(\omega_0, \Delta\tau)(1-K_{1,n}^2)) & \dots & \exp(-\varphi(\omega_0, (NT-1)\Delta\tau)(1-K_{n,n}^2)) \\ \exp(-\varphi(\omega_1, 0)(1-K_{0,n}^2)) & \exp(-\varphi(\omega_1, \Delta\tau)(1-K_{1,n}^2)) & \dots & \exp(-\varphi(\omega_1, (NT-1)\Delta\tau)(1-K_{n,n}^2)) \\ \vdots & \vdots & \dots & \vdots \\ \vdots & \vdots & \dots & \vdots \\ \exp(-\varphi(\omega_{NT-1}, 0)(1-K_{0,n}^2)) & \exp(-\varphi(\omega_{NT-1}, \Delta\tau)(1-K_{1,n}^2)) & \dots & \exp(-\varphi(\omega_{NT-1}, (NT-1)\Delta\tau)(1-K_{n,n}^2)) \end{pmatrix} \quad (\text{A15})$$

\vec{K} is a (N \times 1) vector, M is a (N \times N) matrix and \vec{r} is a (N \times 1) vector. Let \vec{K} be the desired seismic output data while the actual output from Eq. (A14) is $\vec{S} = M \vec{r}$. We want to compute a reflectivity per depth unit series \vec{r} such that the difference $\vec{\Sigma}$ between the actual output \vec{S} and the predicted seismic output data \vec{K} is minimum in the least square sense. Therefore, the error $\vec{\Sigma}$ with respect to parameter vector \vec{r} is $\vec{\Sigma} = \vec{K} - \vec{S} = \vec{K} - M\vec{r}$. And the cumulative squared error:

$$\begin{aligned} \vec{\Sigma}^T \vec{\Sigma} &= (\vec{K} - M\vec{r})^T * (\vec{K} - M\vec{r}) = \\ &(\vec{K}^T * \vec{K} - \vec{K}^T M\vec{r}) - \vec{r}^T M^T K^T + (\vec{r}^T M^T * M\vec{r}) \end{aligned} \quad (\text{A16})$$

Where T denotes matrix transpose and * denotes complex conjugate.

We want to estimate a reflectivity per depth unit series \vec{r} such that the quantity $\vec{\Sigma}^T \vec{\Sigma}$ is minimum. This condition leads to setting the derivative of $\vec{\Sigma}^T \vec{\Sigma}$ with respect to \vec{r} to zero. Differentiate both sides of eq. (A16) with respect to \vec{r} and observe the requirement for least square procedure minimization that

$$\frac{\delta \vec{\Sigma}^T \vec{\Sigma}}{\partial \vec{r}} = -\vec{K}^T * M + \vec{r}^T * M^T * M = 0 \quad (\text{A17})$$

Because \vec{r}^{T*} is complex valued, $\frac{\delta \vec{r}^{T*}}{\delta \vec{r}} = 0$. Thus applying matrix transpose and rearranging the terms of eq. (A17)

$$\begin{aligned} (M^T * M)^T * \vec{r} &= M^T \vec{K} \Rightarrow (M^T M) \vec{r} = M^T * \vec{K} \\ \Rightarrow \vec{r} &= (M^T * M)^{-1} M^T \vec{K} \end{aligned} \quad (A18)$$

Eq (A18) will give us the reflectivity per depth unit and from this we can calculate the impedance.

Damping constant when calculating reflectivity

To further understand the inversion we need to discuss how reflectivity per depth unit is computed and the introduction of the matrix M defined in Eq.(A14). However an important aspect must be discussed first. The singularity of the matrix $M^T * M$ makes it necessary to introduce a damping constant λ when calculating r. This λ is chosen out from the ‘singular value decomposition’ (svd) of the matrix $M^T * M$. Now we get an invertible new matrix:

$$L = \text{svd}(M^T * M) \text{ giving } M^T * M + \lambda I$$

I is a unitary matrix of the same order as the matrix $M^T * M$

$$\begin{aligned} (M^T * M)^T * \vec{r} &= M^T \vec{K} \Rightarrow (M^T M) \vec{r} = M^T * \vec{K} \\ \Rightarrow \vec{r} &= (M^T * M)^{-1} M^T \vec{K} \end{aligned} \quad (A.19)$$

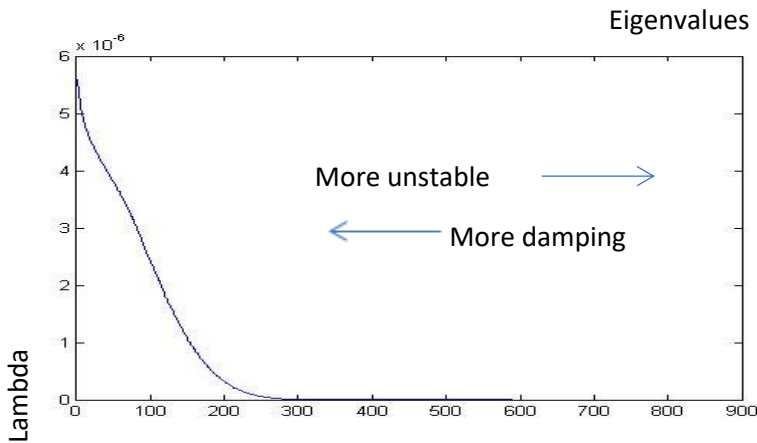


Fig.A.1 .Damping constant lambda as a function of the eigenvalues of $M^T * M$

We will choose lambda around (NT/2) eigenvalue of the matrix $M^T * M$ to be able to use it in the inversion. The output reflectivity (r) will then depend on the value of lambda and introduce damping.

Fig.A.1 shows that when we choose smaller eigenvalues lambda will increase and r is more damped. When lambda increase we found that the effect of the inversion was less and over a threshold value no effect at all. When we increase eigenvalues, lambda decrease. Then we get less damping but r is also more unstable, and can introduce noise. For all calculations in our article we choose lambda=4.8.

It should be taken care to choose the right damping constant (λ) in order to perform the inversion. The choice must be related to noise level, choice of Butterworth filtering and scaling until one gets a satisfying result. We have not discussed this here, but plan to do it in future research.